Low-frequency nonlinear magnetic response of an unconventional superconductor

Igor Žutić* and Oriol T. Valls†

School of Physics and Astronomy and Minnesota Supercomputer Institute, University of Minnesota, Minneapolis, Minnesota 55455-0149
(Received 3 April 1998)

We consider an unconventional superconductor in a low-frequency harmonic magnetic field. In the Meissner regime at low temperatures a nonlinear magnetic response arises from quasiparticle excitations near minima in the energy gap. As a consequence various physical quantities acquire higher harmonics of the frequency of the applied ac field. We discuss how an examination of the field and angular dependences of these harmonics allows the determination of the structure of the energy gap. We show how to distinguish nodes from small finite minima (''quasinodes''). Gaps with nodal lines give rise to universal power-law field dependences for the nonlinear magnetic moment and the nonlinear magnetic torque. They both have separable temporal and angular dependences. In contrast, with gap functions which only have quasinodes, these physical quantities do not display power laws in the applied field, and their temporal and angular dependences are no longer separable. We illustrate this via the example of the nonlinear magnetic moment for a $d+is$ gap. We discuss how to perform ac measurements so as to maximize the nonlinear signal, and how to investigate in detail the properties of the superconducting minima, thus determining the gap function symmetry. [S0163-1829(98)04137-X]

I. INTRODUCTION

There are strong indications from numerous experimental results and theoretical calculations that the symmetry of the pairing state[1-4] in various superconducting materials is not that of an isotropic s wave. Unconventional pairing states have been assigned to different high-temperature superconductors (HTSC's), heavy fermions[5,6] (HF's), and some organic charge transfer salts[7-9] (OS's). The interest in determining the pairing state for these materials arises both from the efforts to obtain significant clues about the microscopic mechanisms responsible for superconductivity and to better understand their physical properties.

For HTSC's it is widely accepted that most of the experimental results support a predominantly d-wave symmetry. There is, however, no consensus about the presence of admixtures of pairing states of different symmetry which would modify the position and value of the minima in the superconducting energy gap. These admixtures might cause the angle between the nodal lines to depart from $\pi/2$ or convert the nodes to very deep minima (''quasinodes''), or both. Part of the difficulty results from the surface character of many high quality pairing state probes. They measure information about the order parameter (OP) within a length scale of a few coherence lengths and are very susceptible to material imperfections near the surface. Furthermore it is not clear whether the pairing states are the same in the surface region as they are throughout the bulk.[10-14] There are also indications that the symmetry of the OP might be temperature dependent.[15-17] The pairing state controversy for other suggested unconventional superconductors such as HF, SrRu$_2$O$_4$,[18,19] and some OS's is even more ambiguous.

In this paper we consider the low-frequency magnetic response of a spin singlet unconventional superconductor in a *time-dependent* magnetic field. We focus on the low-temperature regime in the Meissner state for OP's having lines of nodes (or quasinodes.) The nonlinear response[20-28] arising from quasiparticle excitations near the minima in the

energy gap generates in various physical quantities higher harmonics[29] of the applied field frequency. Since the response extends over a length scale on the order of penetration depth, it constitutes a bulk probe of the superconducting OP. The use of the nonlinear response to a time-independent field to perform gap spectroscopy (that is, to locate the nodes or quasinodes in the gap) was previously discussed.[25] However, nonlinear effects are best detected through the use of ac techniques, since then the nonlinear response takes place at frequencies different from the input frequency at which the much larger linear response is found. These techniques significantly simplify the process of resolving the desired small nonlinear signal, which is a signature of the symmetry of the energy gap, from the large spurious but linear effects such as demagnetization factors, a-b plane penetration depth anisotropy, and trapped flux.

In Sec. II we solve the nonlinear Maxwell-London equations in the low-frequency Meissner regime. We generalize the perturbation method of Ref. 25 to include the temporal dependence. The method is illustrated in the example of an OP with mixed $d+s$ symmetry. We investigate the time and angular dependence of the nonlinear magnetic moment and the associated torque. The results for these quantities are easily extended to other forms of energy gaps with nodes since, as we shall see, in those cases one has separable temporal and angular dependences. The time dependence for gaps with lines of nodes is universal: $H_a(t)|H_a(t)|$ for the nonlinear magnetic moment and $|H_a(t)|^3$ for the nonlinear magnetic torque, where $H_a(t)$ is the applied magnetic field. Both of these quantities have the same angular dependence. The nonlinear effects that we discuss here can also be viewed as field- and angle-dependent corrections to the superfluid density (penetration depth). We briefly discuss how our methods are suitable to extend studies of intermodulation and harmonic generation[29] to low temperatures.

In Sec. III we consider superconducting gaps without nodes but with quasinodes, as illustrated by a $d+is$ OP with a small s component. We examine the nonlinear magnetic

moment, which exhibits a more complicated temporal and angular dependence and a sharp enhancement of its maximum amplitude, compared to that occurring in the case of gaps with nodes. We show how to use these effects to experimentally distinguish nodes from small minima in the superconducting gap. In the final section we present our conclusions and discuss possible extensions of this work.

II. NONLINEAR MAGNETIC RESPONSE

A. Maxwell-London electrodynamics

In the low-frequency regime, i.e., in the quasistatic case,[29–31] the relevant equations of the nonlinear Maxwell-London electrodynamics are formally the same as in the static case. Following the notation and results of the static or dc case,[25] we have

$$\nabla \times \nabla \times \mathbf{v} = \frac{4\pi e}{c^2} \mathbf{j}(\mathbf{v}), \qquad (2.1)$$

where the gauge invariant condensate flow field or superfluid ''velocity'' $\mathbf{v}$ is defined as

$$\mathbf{v} = \frac{\nabla \chi}{2} + \frac{e}{c} \mathbf{A}, \qquad (2.2)$$

with χ the phase of the superconducting singlet OP, $\mathbf{A}$ the vector potential, and e the proton charge. The relation between $\mathbf{j}$ and $\mathbf{v}$ is generally nonlinear and given by[22,23,25]

$$\mathbf{j}(\mathbf{v}) = -e N_f \int_{FS} d^2 s\, n(s) \mathbf{v}_f \Big\{ (\mathbf{v}_f \cdot \mathbf{v}) + 2 \int_0^\infty d\xi f[E(\xi) + \mathbf{v}_f \cdot \mathbf{v}] \Big\}, \qquad (2.3)$$

where N_f is the total density of states at the Fermi level, $n(s)$ the density of states at point s at the Fermi surface (FS) normalized to unity, $\mathbf{v}_f(s)$ the s-dependent Fermi velocity, f the Fermi function with $E(\xi) = (\xi^2 + |\Delta(s)|^2)^{1/2}$, T the absolute temperature, and $\Delta(s)$ the OP. The first term in Eq. (2.3) represents the supercurrent arising from the unperturbed condensate and the second is due to quasiparticle excitations. At $T \approx 0$, and for lines of nodes (or quasinodes), the second term of Eq. (2.3) can be written as[25,32]

$$\mathbf{j}_{qp}(\mathbf{v}) = \sum_n \mathbf{j}_{qp,n}(\mathbf{v}) \approx -2e \sum_n N_{fn} \int_{\Omega_n} \frac{d\phi_n}{2\pi} \mathbf{v}_{fn}[(\mathbf{v}_{fn} \cdot \mathbf{v})^2 - |\Delta(\phi_n)|^2]^{1/2}, \quad n = 1,2,\ldots, \qquad (2.4)$$

where n labels the nodes (quasinodes) of the gap, Ω_n denote regions where quasiparticle excitations are allowed, defined by $|\Delta(\phi_n)| + \mathbf{v}_f \cdot \mathbf{v} < 0$, ϕ_n is the azimuthal angle with respect to the closest node n, and $v_f \approx v_{fn}$ is its value at that node. N_{fn} is the appropriate weighted density of states,[33] equal to N_f for an isotropic FS.

As stated in Ref. 29, the relation between $\mathbf{j}$ and $\mathbf{v}$ given by Eq. (2.3) can be used in the time-dependent case provided that the frequencies are smaller than the quasiparticle relaxation rate. For YBa$_2$Cu$_3$O$_{7-\delta}$ (YBCO), this rate ranges[34,35] from 10^{11} to 10^{13} Hz, depending on the temperature. Mea-

surements of the low-frequency nonlinear magnetic response are designed to be performed[36] at frequencies under 100 Hz, well below this limit.

For different OP's, we study the dependence of the nonlinear magnetic response on the direction of the field applied in the a-b plane. We consider a slab sample, infinite in the a-b plane and of thickness d, much larger than the in-plane penetration depth,[37] in the c direction. This allows for an analytic solution and preserves the angular dependence of the nonlinear effects found for realistic finite three dimensional geometry.[23,24] For a slab, Eq. (2.1) can be written as

$$\partial_{zz} \mathbf{v} + \frac{4\pi e}{c^2} \mathbf{j}(\mathbf{v}) = 0 \qquad (2.5)$$

and the boundary conditions are

$$\mathbf{H}(z,t) = \mathbf{H}_a(t)|_{z = \pm d/2}. \qquad (2.6)$$

We take a particular time dependence of the applied field,

$$H_a(t) = H_{dc} + H_{ac} \cos \omega t, \qquad (2.7)$$

which is suitable to experimentally study higher harmonics arising from the nonlinear response. The parity of quantities such as j_{qp} under a sign change of $H_a(t)$, as it occurs in an ac field, must be carefully taken into account. For an OP satisfying $|\Delta(-\mathbf{k}_f)| = |\Delta(\mathbf{k}_f)|$, where $\mathbf{k}_f$ is the Fermi wave vector, and for $\mathbf{H}_a$ chosen such that the nodal direction of quasiparticle excitations is $\hat{x}_n$, the key point is that a reversed field $-\mathbf{H}_a$ produces excitations along the opposite direction $-\hat{x}_n$. Therefore j_{qp} is odd. This will help us to anticipate various modifications of the results for the static case.

B. Gaps with nodes

We consider an energy gap which can be accurately approximated near its nodes[22,25] by

$$|\Delta(\phi_n)t| \approx |\mu \Delta_{eff} \phi_n|, \quad n = 1,2,\ldots, \qquad (2.8)$$

where μ is the slope of the dominant OP component and Δ_{eff} is the effective amplitude of the gap function. A particular case of Eq. (2.8) corresponds to a $d \pm s$ OP of the form $\Delta_{d\pm s}(\phi) = \pm \Delta_s + \Delta_d \sin 2\phi$, where ϕ is measured from the X axis, depicted in Fig. 1. This form is often chosen to include the effects of orthorhombic distortion in the YBCO family of cuprates, with $\mu = 2$ and $\Delta_{eff} = (\Delta_d^2 - \Delta_s^2)^{1/2}$. For $\Delta_s \neq 0$, the nodes of Eq. (2.8) are no longer separated by an angle of $\pi/2$. The nodal directions are along the unit vectors $\hat{x}_n$, $n = 1,2,\ldots$, which form nonorthogonal axes. The nodes are shifted by an angle $\pm \nu$ (see Fig. 1),

$$\nu \equiv \frac{1}{2} \sin^{-1}\left(\frac{\pm \Delta_s}{\Delta_d} \right), \qquad (2.9)$$

from the orthogonal axes, which we denote by X and Y (the $\pm$ sign corresponds to the $d \pm s$ forms of the gap). Throughout this paper the X and Y axes will remain along the nodal directions of a pure d wave. The direction of the applied field will be given by the angle ψ between $\mathbf{H}_a(t=0)$ and the $+Y$ axis, depicted in Fig. 1. It is convenient to introduce dimen-
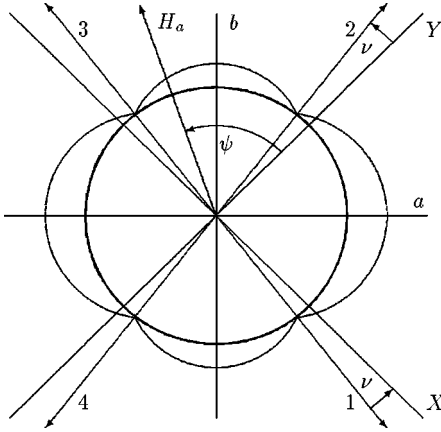
FIG. 1. Coordinates and definitions used in the paper. The FS and the energy gap are shown schematically. The crystallographic directions a and b are indicated. The orthogonal X and Y axes are along the nodal directions of the pure d-wave gap. The $d+s$ nodal directions, labeled 1,2,3,4 are shifted by an angle $\pm\nu$ [see Eq. (2.9)] from their $\Delta_s=0$ values. The applied magnetic field $\mathbf{H}_a$ forms an angle ψ with the $+Y$ direction.

sionless versions of the superfluid velocity and magnetic field. For simplicity, we will perform our calculations below for an isotropic FS. Our results are largely independent of this assumption, as we will occasionally emphasize. It is, however, straightforward to extend these considerations and examine in detail the effects of FS and a-b plane penetration depth anisotropy as have been addressed in Ref. 25. We define

$$u_i \equiv \frac{v_i v_f}{\mu \Delta_{\text{eff}}}, \quad i=X,Y, \qquad (2.10a)$$

$$h_{\text{dc,ac}} = \frac{H_{\text{dc,ac}}}{H_0}, \quad H_0 = \frac{c\Delta_{\text{eff}}}{e\lambda_{ab}v_f}, \quad h=h_{\text{dc}}+h_{\text{ac}}, \qquad (2.10b)$$

where the in-plane penetration depth λ_{ab} for a cylindrical FS is given by $2\pi N_f v_f^2/c^2$. In terms of these quantities and of the dimensionless coordinate $Z \equiv z/\lambda_{ab}$, we obtain, from Eqs. (2.4), (2.5), and (2.10),

$$\partial_{ZZ}u_i - u_i + \text{sgn}[h(t)][e_{1i}(\psi)u_X^2 + e_{2i}(\psi)u_X u_Y + e_{3i}(\psi)u_Y^2]$$

$$=0, \quad i=X,Y, \qquad (2.11)$$

where the factor $\text{sgn}[h(t)]$ arises from the odd parity of j_{qp} with respect to $h(t)=h_{\text{dc}}+h_{\text{ac}}\cos\omega t$ and the constants $e_{1,2,3\,i}(\psi)$ are defined in Appendix A. The appropriate boundary conditions for Eq. (2.11) are

$$\partial_Z u_X|_{Z=Z_s} = \frac{h(t)}{\mu}\cos\psi, \quad \partial_Z u_Y|_{Z=Z_s} = \frac{h(t)}{\mu}\sin\psi,$$

$$u_{X,Y}|_{Z=0} \equiv 0, \qquad (2.12)$$

where $Z_s \equiv d/2\lambda_{ab}$. The solution of Eqs. (2.11) and (2.12) can be sought in the form

$$u_i(Z,t)=u_{i0}(Z)+\sum_j [u_{ij}^e(Z)\cos j\omega t + u_{ij}^0(Z)\sin j\omega t]$$

$$j=1,2,\dots. \qquad (2.13)$$

Using a perturbation method[25] and taking into account the smallness of h_{ac} and h_{dc} by neglecting cubic and higher terms in these parameters, we obtain the leading contribution to $u_i(Z,t)$ (determined by u_{i0}, u_{i1}^e, and u_{i2}^e). The quantities of interest, e.g., the magnetic moment or magnetic torque, can be written down[25] in terms of the surface values of the fields. By substituting Eq. (2.13) into Eqs. (2.11) and (2.12) we get

$$u_i(Z_s,t)=h(t)[\cos\psi\,\delta_{iX}+\sin\psi\,\delta_{iY}]+\frac{h(t)|h(t)|}{3\mu^2}[e_{1i}\cos^2\psi$$

$$+e_{2i}\cos\psi\sin\psi+e_{3i}\sin^2\psi], \quad i=X,Y, \qquad (2.14)$$

where δ_{ij} is the Kronecker symbol. The angular dependence of the second term, nonlinear and nonanalytic in the field, is identical to that found in the case of constant applied field. Thus it remains to investigate the temporal dependence of various quantities which are also nonanalytic. The nonlinear transverse magnetic moment for gaps with nodes can be written (Appendix A) as

$$m_\perp(\psi,t)=\frac{S\lambda_{ab}}{6\mu\pi}\frac{H_a(t)|H_a(t)|}{H_0}\{e_{3X}\sin^3\psi - e_{1Y}\cos^3\psi$$

$$+\cos\psi\sin\psi[(e_{1X}-e_{2Y})\cos\psi$$

$$+(e_{2X}-e_{3Y})\sin\psi]\}$$

$$\equiv N_m \frac{h(t)|h(t)|}{h^2}f(\psi) \equiv N_m \mathcal{M}_\perp(\psi,t), \qquad (2.15)$$

where S is the slab area and the factor λ_{ab} reflects that the nonlinear effects arise from currents present within a length scale on the order of penetration depth. We have introduced the normalization factor

$$N_m = \frac{S\lambda_{ab}(H_{\text{dc}}+H_{\text{ac}})^2}{6\mu\pi H_0}\frac{1}{3\sqrt{3}} \qquad (2.16)$$

and the normalized transverse moment $\mathcal{M}_\perp$. The angular dependence of $m_\perp(\psi,t)$ or of $\mathcal{M}_\perp(\psi,t)$ is given by the function

$$f(\psi)=3\sqrt{3}\{e_{3X}\sin^3\psi - e_{1Y}\cos^3\psi$$

$$+\cos\psi\sin\psi[(e_{1X}-e_{2Y}+(e_{2X}-e_{3Y})]\sin\psi\}. \qquad (2.17)$$

This result is independent of time and thus it is the same as in the static case. For a pure d wave $f(\psi)$ has a maximum value of unity, and so does the normalized moment as a function of angle.

Experimentally, one can best detect the nonlinear effects by examining the dominant harmonics (time Fourier components) of $m_\perp(\psi,t)$, which are at 2ω and 3ω. Analysis of the field and angular dependence of these harmonics makes it possible to accurately determine the position of the nodes in

the energy gap. One could obtain the same information from $m_\parallel(\psi,t)$, discussed in Appendix B, but with greater difficulty because of the extremely large linear signal. The angular dependence of $m_\parallel(\psi,t)$ is different than that of $m_\perp(\psi,t)$ but they both have identical temporal dependence.

Since the measurements are performed in the Meissner state, one must have $H_a(t) \lesssim H_{f1}$, where H_{f1} is the field of first flux penetration, somewhat larger than H_{c1}. Therefore, one wishes to optimize the experimental signal (i.e., the size of the 2ω or 3ω harmonics), by an appropriate choice of the ac and dc components of the applied field at constant total maximum field. We can determine the optimal field mixture, i.e., the ratio $R \equiv H_{dc}/H_{ac} = h_{dc}/h_{ac}$ (at *fixed* total field $h = h_{dc} + h_{ac}$) which would produce the maximum signal for a normalized harmonic $M_j(\psi)$,

$$M_j(\psi) = \frac{2}{\pi(1+\delta_{j0})} \int_0^\pi \frac{m_\perp(\psi,t)}{N_m} \cos j\omega t\, d(\omega t)$$

$$= \frac{2}{\pi(1+\delta_{j0})} \int_0^\pi \frac{h(t)|h(t)|}{h^2} \cos j\omega t\, d(\omega t) f(\psi)$$

$$\equiv \bar{M}_j f(\psi), \quad j = 0,1,2,\dots, \qquad (2.18)$$

which factorizes into field- and angular-dependent parts $\bar{M}_j$ and $f(\psi)$. This factorization is also valid for an anisotropic FS. The field and angular dependence of $m_\perp$ for an anisotropic FS with nodal lines, as obtained in Ref. 25, remains separable in a time varying applied field. As in the static case, FS anisotropy modifies the specific form of $f(\psi)$ but not the field dependence of the coefficient $\bar{M}_j$, provided only that the characteristic field H_0 is properly redefined. Therefore, the determination of the optimal R discussed below would remain the same.

Since the angular dependence $f(\psi)$ is separable, determining the optimal field ratio R reduces to evaluating the coefficient $\bar{M}_j$, the harmonic of the normalized angular amplitude of the nonlinear transverse magnetic moment. The normalizations chosen imply that in the static case, $\omega \to 0$, $\bar{M}_0$ is unity. For $j=2,3$ we obtain from Eq. (2.18)

$$\bar{M}_2 = \frac{1}{\pi h^2}\left[h_{ac}^2 p + 4 h_{dc} h_{ac}\left(\cos p - \frac{\cos 3p}{3} \right) \right.$$

$$\left. - (2h_{dc}^2 + h_{ac}^2)\sin 2p + \frac{h_{ac}^2}{4}\sin 4p \right], \qquad (2.19a)$$

$$\bar{M}_3 = \frac{1}{\pi h^2}\left[h_{ac}^2 \cos p - \left(\frac{4}{3}h_{dc}^2 + \frac{2}{3}h_{ac}^2 \right)\cos 3p + \frac{h_{ac}^2}{5}\cos 5p \right.$$

$$\left. - h_{dc} h_{ac}(2\sin 2p - \sin 4p) \right], \qquad (2.19b)$$

where $p \equiv \sin^{-1}(h_{dc}/h_{ac})$. Results for $\bar{M}_2$ and $\bar{M}_3$ at fixed maximum field as a function of the ratio R are given in Fig. 2. We show results for $H_{dc} < H_{ac}$ ($R<1$) only, since for
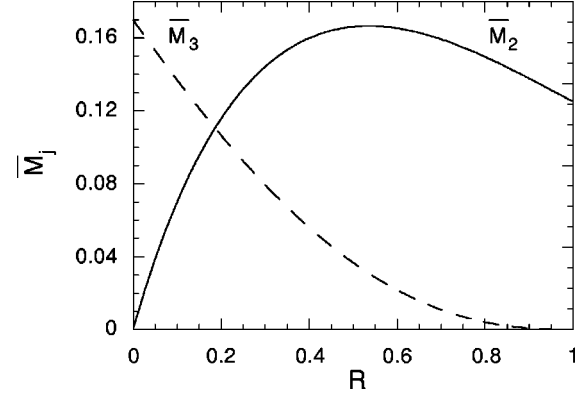

FIG. 2. Harmonics, $\bar{M}_j$, $j=2,3$, at 2ω, 3ω of the normalized transverse magnetic moment angular amplitude [Eq. (2.18)], plotted as a function of the field ratio $R \equiv h_{dc}/h_{ac}$. Normalization is taken so that in the static case, $\omega \to 0$, $\bar{M}_0$ is unity.

larger values of R these harmonics are considerably smaller. The results indicate that the optimal applied field should be a pure ac field if the harmonic at 3ω is measured, or $H_{ac} \approx 2H_{dc}$ for the 2ω harmonic. If one measures these harmonics for several values of R close to optimal, their dependence on R, as we shall see in Sec. III, can serve to experimentally distinguish nodes from small minima in the energy gap. The reduction of the amplitude for $\bar{M}_j$, $j=2,3$, compared to the static case (a factor of ≈ 6) is more than compensated by the advantages of ac techniques.[38]

We can apply a similar analysis to the magnetic torque, $\boldsymbol{\tau} = \mathbf{m} \times \mathbf{H}$. Torque magnetometry is an extremely sensitive experimental technique, which has already been used to investigate anisotropic magnetic properties of superconductors at higher fields.[39–41] Here we are interested in τ_z, which has an angular dependence identical to that of $m_\perp(\psi)$. The main harmonics arising from the nonlinear response are at 3ω and 4ω. Using a convention similar to that in Eq. (2.18) we define

$$T_j(\psi) = \frac{2}{\pi}\int_0^\pi \frac{|h(t)|^3}{h^3} \cos j\omega t\, d(\omega t) f(\psi) \equiv \bar{T}_j f(\psi), \quad j=3,4,$$

$$(2.20)$$

where we make use of the separability of the angular dependence. To determine the optimal R we need only consider $\bar{T}_j$, the harmonic of normalized angular amplitude of the nonlinear torque. Elementary integration in Eq. (2.20) yields

$$\bar{T}_3 = \frac{1}{\pi h^3}\left[\frac{h_{ac}^3}{2}p + 3 h_{dc} h_{ac}^2 \cos p - \left(\frac{4}{3}h_{dc}^3 + 2 h_{dc} h_{ac}^2 \right)\cos 3p \right.$$

$$+ \frac{3}{5}h_{dc} h_{ac}^2 \cos 5p - \left(3 h_{dc}^2 h_{ac} + \frac{3}{4}h_{ac}^3 \right)\left(\sin 2p - \frac{\sin 4p}{2} \right)$$

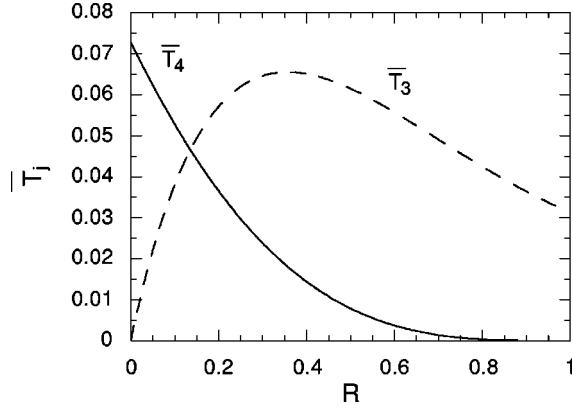$$\left. - \frac{h_{ac}^3}{12}\sin 6p \right], \qquad (2.21a)$$

FIG. 3. Harmonics, $\bar{T}_j$, $j=3,4$, at 3ω, 4ω of the normalized magnetic torque amplitude [Eq. (2.20)], as a function of $R \equiv h_{dc}/h_{ac}$. Results are shown for gaps with lines of nodes. Normalization is as in Fig. 2.

$$\bar{T}_4 = \frac{1}{\pi h^3}\left[\frac{h_{ac}^3\cos p}{2} - \left(2h_{dc}^2 h_{ac} + \frac{h_{ac}^3}{2}\right)\cos 3p\right.$$

$$+\left(\frac{6}{5}h_{dc}^2 h_{ac} + \frac{3}{10}h_{ac}^3\right)\cos 5p - \frac{h_{ac}^3}{14}\cos 7p - \frac{3}{2}h_{dc}h_{ac}^2$$

$$\left.\times \sin 2p + \left(h_{dc}^3 + \frac{3}{2}h_{dc}h_{ac}^2\right)\sin 4p - \frac{h_{dc}h_{ac}^2}{2}\sin 6p\right].$$

$$(2.21b)$$

The results for $\bar{T}_j$ as a function of R at fixed maximum field, seen in Fig. 3, show that for gaps with nodes it is optimal to measure the 4ω time Fourier component (FC) at pure ac applied field, and the 3ω component at $R \approx 0.35$. As in our discussion of $\bar{M}_j$, one can see that FS anisotropy does not alter $\bar{T}_j$ or the optimal value of R.

C. Microstrip resonator

The nonlinear aspects we discuss here affect many other frequency-dependent phenomena. We refer here briefly as an example to the nonlinear magnetic response of a microstrip resonator at low temperature. The particular geometry is that from Ref. 29 where the nonlinear dynamics was discussed for higher temperatures, when the relation between $\mathbf{j}$ and $\mathbf{v}$ is analytic. At low temperature the effect is quite different, as the nonlinearities are nonanalytic. For a cylindrical, isotropic FS, Eq. (2.3) can be expressed as

$$\mathbf{j} = -e\rho\mathbf{v} + \mathbf{j}_{qp} = -e\tilde{n}_s\mathbf{v}, \qquad (2.22)$$

where we use a notation distinguishing the electron density ρ from the superfluid density tensor $\tilde{n}_s$, which also includes anisotropic, nonlinear effects due to quasiparticle excitations. The specific form of $\tilde{n}_s$ depends on the angular form of the energy gap and can be simply obtained from j_{qpi} in Eq. (A1). The effects that we investigate can be viewed as arising either from a time-dependent applied magnetic field or a driven time varying current. Following Ref. 29, we consider

a pure d-wave gap with an applied field (or driven current) along nodal and antinodal directions. In both cases $\mathbf{j}\|\mathbf{v}$. We have

$$\frac{\lambda^2(T=0, \mathbf{j}=0)}{\lambda^2(0,\mathbf{j})} = \frac{n_s(0,\mathbf{j})}{n_s(0,0)} = 1 - b_\psi\frac{|\mathbf{j}|}{|j_c|}, \qquad (2.23)$$

where $\psi=0$ corresponds (Fig. 1) to $\mathbf{j}$ along the nodal and $\psi=\pi/4$ to $\mathbf{j}$ along the antinodal direction. From Appendix A we obtain $b_{\psi=0}=1/2$ and $b_{\psi=\pi/4}=1/2\sqrt{2}$. The critical current is $j_c = n_s(0,0)e\Delta_d/v_f$ and in the absence of quasiparticle excitations at $T=0$, $j=0$, the superfluid density $n_s(0,0)$ equals ρ.

We next examine the inductance per unit length L and show how the low-temperature form of $\mathbf{j}(\mathbf{v})$ affects its nonlinear corrections. These considerations are then readily applied to other quantities of interest such as the resistance per unit length or the quality factor Q. We use the expression for the inductance[29]

$$L = \frac{\int_S [H^2 + \lambda^2(0,j)(4\pi j/c)^2]dS}{4\pi\left(\int_S j\,dS\right)^2} \qquad (2.24)$$

with the integration being over a cross section of the microstrip having width w and thickness d. This expression can be rewritten as

$$L = L_0 + \Delta L\frac{|I|}{|I_c|}, \qquad (2.25)$$

where L_0 is the inductance in the linear response, $I = \int_S j\,dS$, and $I_c\int_S j_c dS = wdj_c$. We make the approximation[29] that the total correction ΔL due to the nonlinear response can be replaced by the kinetic part only, ΔL_{KI}. Then, by using Eqs. (2.23)–(2.25) we obtain $L\approx L_0 + \Delta L_{KI}|I|/|I_c|$ with

$$\Delta L_{KI} = \frac{4\pi b_\psi\lambda^2(0,0)wd\int_S|j^3|dS}{c^2\left|\int_S j\,dS\right|^3}. \qquad (2.26)$$

One can consider also the frequency-dependent Q or the resistance, which can be decomposed into linear and nonlinear parts as in Eq. (2.25). The power-law behavior of the nonlinear corrections in these quantities, i.e., linear in I/I_c [instead of $(I/I_c)^2$ at higher temperatures] will affect generation of higher harmonics. By using the transmission line equations[29] for a microstrip, one easily sees that these two types of nonlinearity give rise to second harmonic generation at low T eventually crossing over to third harmonic at higher temperatures.

III. DETECTION OF NODELESS GAP FUNCTIONS

In this section we investigate the quasistatic nonlinear magnetic response of anisotropic energy gaps with "quasinodes" rather than with nodes. The nonlinear electromagnetism samples the pairing state in the bulk. If the nodes are

absent only in a layer of thickness much smaller than λ near the surface,[12,13] our results from Sec. II apply unmodified. We consider here a typical candidate, $d+is$,[42–44] energy gap with the d component being dominant. The results presented are quite similar to those that can be obtained for other nodeless gaps such as $d_{x^2-y^2}+id_{xy}$ (Refs. 45–47) or an anisotropic s wave. Generally, in the absence of nodes, the analysis of the low-frequency nonlinear magnetic response is more complicated. There are threshold effects that decisively affect the field dependence.

We can approximate a $d+is$ (Refs. 43,44) gap near its minima by

$$|\Delta(\phi_n)| \approx (\mu^2 \Delta_d^2 \phi_n^2 + \Delta_s^2)^{1/2}, \quad n=1,2,\ldots, \quad (3.1)$$

with $\Delta_s \ll \Delta_d$ and $\mu=2$ for the usual form of a d-wave OP. The small minima (Δ_s) are located at the positions of the nodal points in a d-wave gap. The current due to the quasiparticle excitations is obtained from Eq. (2.4)

$$\mathbf{j}_{\mathrm{qp}}(\mathbf{v}) \approx -\frac{e}{2} \sum_n N_f v_f \hat{x}_n \frac{v_f^2 (\mathbf{v}\cdot\hat{x}_n)^2 - \Delta_s^2}{\mu^2 \Delta_d^2} \Theta[v_f^2(\mathbf{v}\cdot\hat{x}_n)^2 - \Delta_s^2],$$

$$n=1,2,\ldots, \quad (3.2)$$

where the step function arises from the phase space for allowed quasiparticle excitations ($|\Delta(\phi_n)| + \mathbf{v}_f \cdot \mathbf{v} < 0$) given by

$$\phi_n^2 \leq \frac{v_f^2 (\mathbf{v}\cdot\hat{x}_n)^2 - \Delta_s^2}{\mu^2 \Delta_d^2}, \quad (3.3)$$

which is reduced compared to the d-wave gap. The step functions result in a threshold effect: it now takes a minimum field to create quasiparticles. However, as we shall later see, a small admixture of s waves in a $d+is$ gap can enhance *the maximum value* of the nonlinear effects at fields above threshold. From Eq. (3.3) it follows that the nonlinear effects are absent whenever $H_a(t)$ is small enough so that $|v| < v_T \equiv \Delta_s/v_f$. In dimensionless form the threshold field h_T and the threshold velocity u_T are

$$h_T \equiv \delta, \quad u_T \equiv \frac{\delta}{\mu}, \quad \delta \equiv \frac{\Delta_s}{\Delta_d}. \quad (3.4)$$

The substitution of Eq. (3.2) into (2.5) yields

$$\partial_{ZZ} u_i - u_i + \mathrm{sgn}[h(t)](u_i^2 - u_T^2)\Theta(|u_i| - u_T) = 0, \quad i=X,Y, \quad (3.5)$$

where u_i is given by Eq. (2.10) with $\Delta_{\mathrm{eff}} = \Delta_d$. By modifying the methods used in this case for a static field[25] to include the time dependence we obtain

$$u_i(Z_s,t) = h(t)[\cos\psi\delta_{iX} + \sin\psi\delta_{iY}]$$

$$+ \left[\frac{1}{3\mu^2}h(t)|h(t)|(\cos^2\psi\delta_{iX} + \sin^2\psi\delta_{iY})\right.$$

$$-u_T^2\mathrm{sgn}[h(t)] + \frac{4u_T^3}{3h(t)(\cos\psi\delta_{iX} + \sin\psi\delta_{iY})}\right]$$

$$\times \Theta\left(|h(t)| - \frac{h_T}{(\cos\psi\delta_{iX} + \sin\psi\delta_{iY})}\right),$$

$$i=X,Y \quad (3.6)$$

for the solution at the surface of a slab, $Z=Z_s$ ($Z_s \gg 1$), which suffices to express the quantities $m_\perp$ and τ_z. Nonlinear effects are present only for $h(t) \geq h_{Ti}(\psi,\delta) \geq h_T$, where $h_{TX} \equiv \delta/\cos\psi$ and $h_{TY} \equiv \delta/\sin\psi$ are the angle-dependent threshold fields required to excite jets of quasiparticles centered along the X and Y axes, respectively. The transverse magnetic moment is

$$m_\perp(\psi,t) = \frac{S\lambda_{ab}}{6\mu\pi}\left[\frac{H_a(t)|H_a(t)|}{H_0}\cos\psi\sin\psi\right.$$

$$\times \{\cos\psi\Theta[|h(t)| - h_{TX}] - \sin\psi\Theta[|h(t)| - h_{TY}]\}$$

$$+ 3\delta^2 H_0\mathrm{sgn}[H_a(t)]\{\cos\psi\Theta[|h(t)| - h_{TY}]$$

$$- \sin\psi\Theta[|h(t)| - h_{TX}]\}$$

$$- 2\delta^3\frac{H_0^2}{H_a(t)}\{\cot\psi\Theta[|h(t)| - h_{TY}]$$

$$\left. - \tan\psi\Theta[|h(t)| - h_{TX}]\right], \quad (3.7)$$

where we see that, as stated above, the temporal and angular dependences of $m_\perp(t,\psi)$ are no longer separable. To investigate the behavior of this expression at different fields and admixtures of s wave OPs it is useful to employ the scaling relation

$$m_\perp[\kappa h(t), \kappa\delta] = \kappa^2 m_\perp[h(t),\delta] \quad (3.8)$$

valid for any angle ψ, at fixed field ratio R. The quantity κ is an arbitrary scaling factor.

Again, we investigate the dominant harmonics of $m_\perp(\psi,t)$. Because of the nonseparability of temporal and angular dependences, one cannot introduce $\bar{M}_j$ as in Eq. (2.18). One must now carefully consider both the harmonics

$$M_j(\psi) = \frac{2}{\pi}\int_0^\pi \frac{m_\perp(\psi,t)}{N_m}\cos j\omega t\, d(\omega t), \quad j=2,3, \quad (3.9)$$

and the relevant angular Fourier components (FC's) in terms of which the angular dependence can be analyzed. The most important angular FC is that which reflects the main angular periodicity $\pi/2$ of the energy gap:

$$M_j^4 = \frac{8}{\pi}\int_0^{\pi/4} M_j(\psi)\sin 4\psi\, d\psi, \quad j=2,3. \quad (3.10)$$

We will focus in the rest of this section on the dominant response of the nonlinear magnetic moment at 2ω and 3ω.
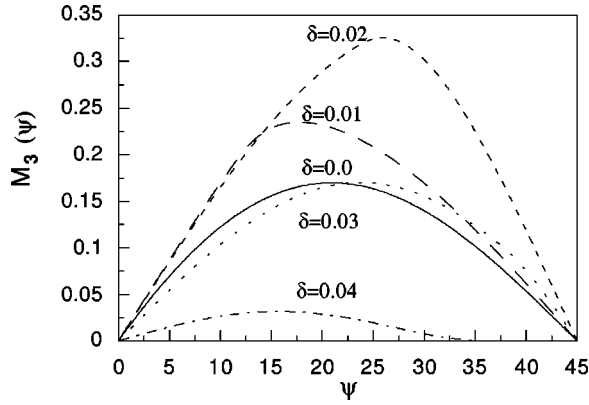
FIG. 4. Angular dependence of $M_3(\psi)$ [see Eq. (3.9)] the 3ω harmonic of the normalized transverse magnetic moment $\mathcal{M}_\perp$ for various admixtures of s waves in a $d+is$ energy gap. Results are shown at $h=h_{ac}=0.05$ and normalized (as in Fig. 2) so that the maximum of $\mathcal{M}_\perp$ for a pure d-wave gap is unity. Lines are labeled by the ratio of s- and d-wave amplitudes, $\delta \equiv \Delta_s/\Delta_d$.

In Fig. 4 we show our results for the angular dependence of the 3ω harmonic $M_3(\psi)$. The details of its calculation are given in Appendix C. We display the range $\psi \in [0,\pi/4]$. We have taken $R=0$ (guided by Fig. 2) and a dimensionless field amplitude $h=h_{ac}=0.05$. This value, using typical material parameters for YBCO, corresponds to $H_{ac} \approx H_{f1}$. The solid line represents the d-wave result, normalized such that the maximum of $\mathcal{M}_\perp(\psi)$ for the static case is unity. This normalization is employed throughout this section. The broken lines are labeled by the corresponding ratios δ.

An obvious feature seen in Fig. 4 is the enhancement of the maximum value of the signal that may arise from small admixtures of an s-wave OP. At fixed field, the maximum enhancement of $M_3(\psi)$ is much more pronounced than the moderate one for $m_\perp(\psi)$ found in the static case (Fig. 7 in Ref. 25). A similar enhancement is also present in $M_2(\psi)$. This result is rather unexpected since such an admixture would reduce the available phase space [recall Eq. (3.3)] for quasiparticle excitations. This enhanced signal is of non-negligible significance in planning experiments. We therefore pause here to explain its physical origin.

The nonlinear transverse magnetic moment arises from contributions due to components of the quasiparticle current $\mathbf{j}_{qp,n}(\mathbf{v})$ at different nodes (quasinodes). These contributions partly cancel each other as each node, in effect, tries to twist the magnetic moment away from itself. Thus, if a magnetic field is applied along an antinode, the cancellation of such components is complete and $m_\perp=0$. To explain the peculiar enhancement in $M_3(\psi)$, we need to investigate how the introduction of Δ_s increases the *asymmetry* of such contributions from different jets. The asymmetry, which is reflected in the angular asymmetry of the curves in Fig. 4 for $\delta>0$, is brought about by one of the nodes being above its angular-dependent threshold field [see below Eq. (3.6)] while the other is still below. It was seen in Ref. 25 that this was responsible for the small enhancement seen in the dc case. Now we will see quantitatively how the larger enhancement in the ac case arises from the same source.

We denote the contributions to $\mathcal{M}_\perp \equiv m_\perp/N_m$ of the individual jets along the X and Y axes at a fixed angle ψ_0 by $\mathcal{M}_\perp(\psi_0,t)_X$, $\mathcal{M}_\perp(\psi_0,t)_Y$:
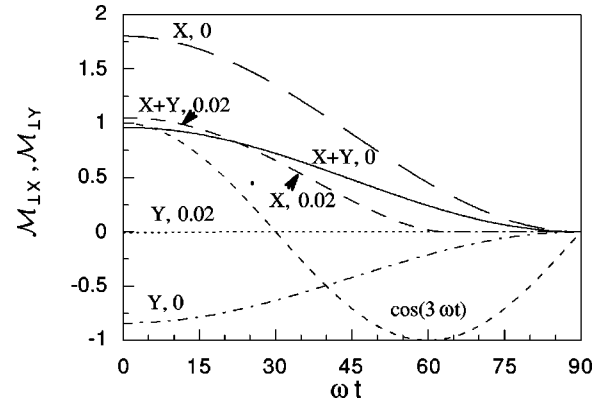

FIG. 5. Time dependence in a $d+is$ state of $\mathcal{M}_\perp(\psi,t)$ [Eq. (3.11)] and its contributions from jets along the X [$\mathcal{M}_\perp(\psi,t)_X$] and Y [$\mathcal{M}_\perp(\psi,t)_Y$] axes. Normalization and field are as in Fig. 4. Results shown are at fixed angle $\psi_0=25°$ for which (Fig. 4) the signal for $\delta=0.02$ is substantially enhanced as compared to the pure d-wave case. Curves are labeled by the axes describing the contribution from a particular jet, and the value of δ. Also shown is $\cos 3\omega t$, which enters the definition of $M_3(\psi)$ in Eq. (3.9) and accounts for part of the enhancement.

$$\mathcal{M}_\perp(\psi_0,t) = \mathcal{M}_\perp(\psi_0,t)_X + \mathcal{M}_\perp(\psi_0,t)_Y. \quad (3.11)$$

In Fig. 5, computed for the same fields as in Fig. 4, we show $\mathcal{M}_\perp(\psi,t)_X$, $\mathcal{M}_\perp(\psi,t)_Y$, and their sum $\mathcal{M}_\perp(\psi,t)$ as a function of time ωt at a fixed angle $\psi \equiv \psi_0 \equiv 25°$ in the region where the maximum of $M_3(\psi;\delta=0.02)$ occurs. We see in Fig. 4 that the enhancement in this case is large, a factor of about 2 over the d-wave signal. The quantities in the figure are shown for both $\delta=0$ and 0.02. The curves are labeled by two indices, the first a letter denoting the jet, or sum of jets, plotted and the second being the value of δ. The range $\omega t \in [0,90°]$ shown in the figure could be extended over the whole period by symmetry. For the chosen value of ψ_0, the threshold fields satisfy $h_{TX}(\psi_0)<h_{TY}(\psi_0)$ and consequently the magnitude of the jet along the X axis is greater than that of the one along the Y axis. With the admixture of an s-wave OP, there is a region $\omega t \lesssim 20°$, where the magnitude of $\mathcal{M}_\perp(\psi_0,t)_X$ is reduced to *less* than that of $\mathcal{M}_\perp(\psi_0,t)_Y$. Therefore the cancellation of the contributions from the two different jets takes place to a lesser extent, resulting in an overall increase of $\mathcal{M}_\perp(\psi_0,t)$. However, this accounts for only part of the enhancement seen in Fig. 4, basically the part found in the dc case, which corresponds to that at $\omega t =0$ in the figure. The remaining part of the increase in $M_3(\psi)$ is explained by the convolution of the time dependence of $\mathcal{M}_\perp(\psi,t)$ and $\cos 3\omega t$ in the definition of $M_j(\psi)$, Eq. (3.9). When the curves representing $m_\perp(\psi,t)$ for $\delta =0,0.02$ and $\cos 3\omega t$ (which is also shown in Fig. 5) are multiplied the results obtained, which are the integrands in Eq. (3.9), are as shown in Fig. 6. The solid curve represents the pure d-wave result and the broken curve that for $\delta =0.02$. The ratio of the two net areas between the curves shown and the horizontal axis is about a factor of 2, i.e., the factor between $M_3(\psi_0)$ for $\delta=0$ and for $\delta=0.02$ in Fig. 4. Thus, the enhancement is explained.

It is straightforward to perform a very similar analysis for $M_2(\psi)$ using its explicit expression from Appendix C. From parity considerations, similar to those made for gaps with
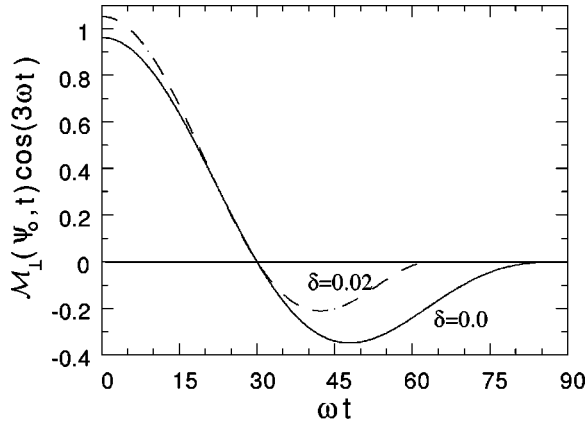
FIG. 6. Origin of the enhancement of $M_3(\psi)$ (the 3ω harmonic of $\mathcal{M}_\perp$) at $h=h_{ac}=0.05$, and $\psi\equiv\psi_0=25°$ (recall Fig. 4) with the admixture of s-wave component in the $d+is$ gap. The curves, which represent the product of the normalized magnetic moment $\mathcal{M}_\perp$ and $\cos(3\omega t)$ (see Fig. 5) are labeled by the corresponding value of δ.

nodes, $M_2(\psi)$ vanishes identically as a function of δ and ψ for $h_{dc}=0$. In this case, one chooses $R\approx0.5$ (see Fig. 2) and again finds an enhanced signal, as in Fig. 4. The size of the enhancement is largely due to the convolution with $\cos 2\omega t$.

The nonseparable temporal and angular dependences of $m_\perp(\psi,t)$ require additional care in trying to determine the optimal mixture of dc and ac fields in $H_a(t)$ which maximizes the harmonics and angle FC's of the signal. From the expressions for $M_2(\psi)$ in Eq. (C1) we have obtained results for its $\pi/2$ angular FC. We denote this quantity by M_2^4, as defined in Eq. (3.10). We show typical results in Fig. 7. There we plot M_2^4 as a function of R at $h=0.05$, for several values of δ. The solid line represents the pure d wave and the broken lines are labeled by their value of δ. We see that the optimal field ratio depends on the particular s-wave admixture. Through the scaling relation in Eq. (3.8) these results can be simply extended to other values of h and δ. In Fig. 8, we plot M_3^4 (i.e., the $\pi/2$ angular FC of the signal at

3ω) as a function of R at maximum dimensionless field $h=0.05$ for the same values of δ. In this case $R=0$ produces the maximal signal, for all δ.

It is instructive, in order to learn how to distinguish nodes from quasinodes, to contrast Fig. 2, which displays $\bar{M}_j$, $j=2,3$, the angular amplitude of the 2ω and 3ω harmonics for a gap with nodes, with Figs. 7 and 8. Because of the separable temporal and angular dependences of $m_\perp(\psi,t)$ when nodes are present, the solid lines (pure d-wave case) in Figs. 7 and 8 are simply proportional (with a normalization factor[48] ≈1) to the curves $\bar{M}_2$ or $\bar{M}_3$, respectively. Experimentally, a sensitive test would be to measure M_2^4, M_3^4 for several values of R, and compare the R dependence with the corresponding solid lines in Figs. 7 and 8. The deviation from these lines would indicate the absence of nodes in the gap. A further way of analyzing such data is suggested by Figs. 9 and 10 where we show M_2^4 and M_3^4, respectively, as functions of δ, for several values of R [additional results are easily obtained using Eq. (3.10) and the expressions in Appendix C]. The curves plotted are labeled by their values of R and are given at a fixed maximum field $h=0.05$. To com-

FIG. 8. Field ratio R dependence of the angular $\pi/2$ Fourier component M_3^4 of the 3ω signal of the normalized transverse magnetic moment $\mathcal{M}_\perp$. Results shown are for various admixtures of s waves in a $d+is$ state at $h=0.05$. Normalization and labeling are the same as in Fig. 7.
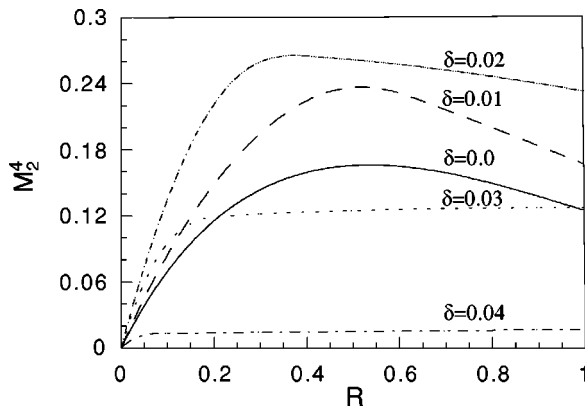

FIG. 7. Field ratio $R\equiv h_{dc}/h_{ac}$ dependence of M_2^4 [the angular $\pi/2$ Fourier component of the 2ω signal of the normalized transverse magnetic moment $\mathcal{M}_\perp$, Eq. (3.10)], for various admixtures of s waves in a $d+is$ energy gap. Results are given at $h=0.05$. The normalization is as in Fig. 4. The curves are labeled by the ratio $\delta=\Delta_s/\Delta_d$ with the same values as in Fig. 4.
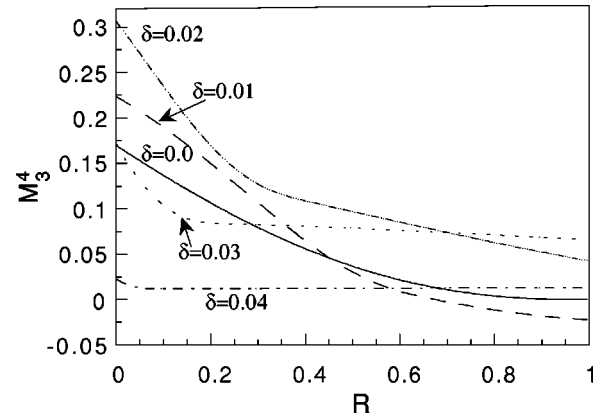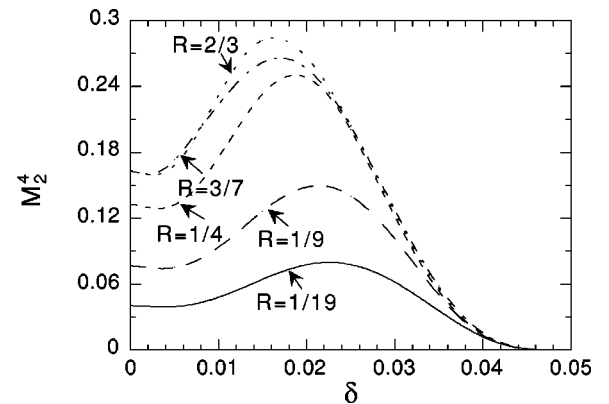

FIG. 9. Dependence of the angular $\pi/2$ Fourier component M_2^4 of the 2ω nonlinear magnetic moment signal $\mathcal{M}_\perp$ (recall Fig. 7) on the admixtures of s-wave components in a $d+is$ gap. Results are shown at $h=0.05$ and normalized as in Fig. 7. Curves plotted are labeled by the corresponding value of R.
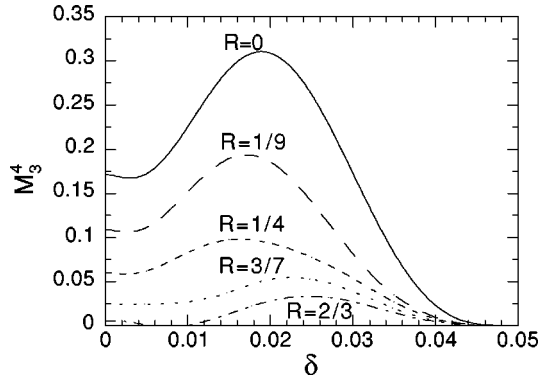
FIG. 10. Dependence of the angular $\pi/2$ Fourier component of the 3ω signal M_3^4 of $\mathcal{M}_\perp$ (compare with Fig. 8) on the admixture of s-wave components in a $d+is$ state. Results are shown at $h=0.05$ and normalized as in Fig. 7. Curves plotted are labeled by their value of R.

pare experimental data with an assumed $d+is$ gap, and to determine the s-wave admixture, one would look for a value of δ which agrees with a particular dependence of the measured M_2^4 or M_3^4 at different R. In these figures we notice again the implications of the nonmonotonic behavior of $m_\perp$ (or $\mathcal{M}_\perp$) with δ. Just as we found above for the harmonics, there is also a substantial enhancement for the angular FC at given R as compared to the $\delta=0$ value. It has the same origin, as shown in Figs. 5 and 6, predominantly due to the convolution of $M_j(\psi,t)$ and $\cos(j\omega t)$, $j=2,3$. In Figs. 9 and 10 we see that maximum such enhancement (at different values of R) is located typically in the range $0.015 \lesssim \delta \lesssim 0.025$ at $h=0.05$. More generally, using the scaling relation Eq. (3.8), for an arbitrary maximum field h (within the Meissner regime) the maximum signal for M_j^4, $j=2,3$ is approximately in the range $h/3 \lesssim \delta \lesssim h/2$.

Thus, there are several distinct features for which the results for a nodeless gap with small minima differ considerably from those for gaps with true nodes. These results suggest how to perform measurements and analyze the nonlinear quantities in the low-frequency, low-temperature regime. They can be supplemented with the results from the static case. It would also be useful to study the field dependence of $m_\perp$ and its Fourier components at fixed R while changing the maximum field ($H_{dc}+H_{ac}$).

Using the methods that we have presented, similar results for the behavior of the nonlinear magnetic torque can be obtained. Analogously, results for other gapped states such as $d_{x^2-y^2}+id_{xy}$ can be derived without difficulty.

IV. CONCLUSIONS

We have examined properties of the nonlinear magnetic response of an unconventional superconductor at low frequencies. There are two key points to our conclusions. First, these frequency-dependent nonlinear phenomena provide a particularly powerful tool to distinguish nodes from quasinodes. Second, the experimental sensitivity that allows one to perform ''node spectroscopy'' can be considerably enhanced over the corresponding dc result.

For gap functions with nodal lines the nonlinear moment ($m_\perp$, $m_\parallel$) and torque (τ_z) have separable field (and hence,

time) and angular dependences. These quantities are respectively quadratic and cubic (up to a sign determined by parity) in the instantaneous applied field. The nonlinear magnetic response for nodeless gaps is more complicated: the time (or field) and angular dependences are not separable and the field dependence is not a simple power law. We have discussed how these features can be studied by measuring higher harmonics (referred to as the frequency of the applied ac field) of various physical quantities. For an applied field $H_a(t)=H_{dc}+H_{ac}\cos\omega t$, at a fixed maximum $H_{dc}+H_{ac}$ we have computed the optimal ratio $R\equiv H_{dc}/H_{ac}$ at which the signal (for a certain higher harmonic) is largest. For gaps with lines of nodes it is most favorable to measure the 2ω harmonic of $m_\perp$ at $R\approx 0.5$ or the 3ω harmonic at $R=0$, while for τ_z the best alternatives are the 3ω harmonic at $R\approx 0.35$ and the 4ω harmonic component at $R=0$. These results are independent of the specific angular dependence of the gaps with nodal lines and are also valid for an anisotropic FS. In the absence of nodes, as we illustrate through the example of a $d+is$ gap, selecting the optimal value of R to maximize higher harmonics is less simple but more rewarding. The result depends on the particular admixture of s-wave component to the OP and hence provides for the quantitative determination of this admixture. The results we have shown are sensitive to the angular position of nodal (quasinodal) lines, allowing for detailed characterization of the minima in the energy gap.

The analysis presented here can be generalized to include point nodes, and to triplet pairing. The field dependence for gaps with point nodes is different than that found for gaps with lines of nodes. For example, $m_\perp$ is cubic rather than quadratic in the instantaneous value of the applied field. Using these considerations and the temperature range attainable by a dilution refrigerator it should be feasible to experimentally study other candidates for unconventional superconductivity, such as heavy fermions, organic superconductors, and $SrRu_2O_4$. Analysis of the material parameters (to estimate H_0 and H_{f1}) shows that in many cases the expected signal should be at least as large as for HTSC's. Experiments investigating magnetic response in these materials, at sub-Kelvin temperatures, are currently under considerations.[49]

APPENDIX A: CURRENTS

Integration of Eq. (2.4) without a-b plane FS anisotropy yields[25]

$$j_{qpi}=\frac{1}{2}eN_f\frac{v_f^3}{\mu\Delta_{eff}}[e_{1i}(\psi)v_X^2+e_{2i}(\psi)v_Xv_Y+e_{3i}(\psi)v_Y^2],$$

$$i=X,Y, \qquad (A1)$$

where the coefficients $e_{1,2,3\,i}(\psi)$ are defined for various ranges of ψ. Depending on the particular orientation of $\mathbf{H}_a$,

as given by the angle ψ, these coefficients describe contributions from different jets. The results are quadratic in the superfluid velocity. For a $d \pm s$ OP we obtain

$$e_{1X} = e_{3Y} = c^3 - s^3,$$

$$e_{2X} = 2e_{3X} = 2e_{1Y} = e_{2Y} = -2cs(c-s),$$

$$\psi \in \left[\nu, \frac{\pi}{2} - \nu \right], \qquad (A2a)$$

$$e_{1X} = -e_{3Y} = -(c^3 + s^3),$$

$$e_{2X} = -2e_{3X} = 2e_{1Y} = -e_{2Y} = 2cs(c+s),$$

$$\psi \in \left[\frac{\pi}{2} - \nu, \pi + \nu \right], \qquad (A2b)$$

where $c \equiv \cos \nu$ and $s \equiv \sin \nu$. The pure d-wave limit corresponds to $c=1$ and $s=0$.

APPENDIX B: MAGNETIC MOMENT FOR A GAP WITH LINES OF NODES

The magnetic moment can be calculated using only the surface values of the fields.[24,25,50] For the geometry considered here, the magnetic moment

$$\mathbf{m} = \frac{1}{2c} \int d\mathbf{r} \, \mathbf{r} \times \mathbf{j}(\mathbf{v}), \qquad (B1)$$

can be expressed as

$$m_{x,y} = - \frac{\mathcal{S} d H_{ax,y}}{4\pi} \mp \frac{\mathcal{S}c}{2\pi e} v_{y,x}(d/2), \qquad (B2)$$

where x and y are orthogonal axes fixed in space, $\mathcal{S}$ is the slab area, and we have used that $\mathbf{v}$ is odd in z. For a slab $(d \gg \lambda_{ab})$, which is the case of experimental interest,[21] the nonlinear magnetic moment can be obtained from $u_i(Z,t)$, given in Eq. (2.14). For a gap with node lines it is $\propto h(t)|h(t)|$. The transverse component $m_\perp = m_X \cos \psi + m_Y \sin \psi$, perpendicular to the applied field, is obtained from Eq. (2.15) and the longitudinal component of the nonlinear magnetic moment $m_\parallel = -m_X \sin \psi + m_Y \cos \psi$ is given by

$$m_\parallel(\psi) = \frac{\mathcal{S} \lambda_{ab}}{6\mu\pi} \frac{H_a(t)|H_a(t)|}{H_0} \{ e_{1X} \sin^3 \psi + e_{3Y} \cos^3 \psi$$

$$+ \cos \psi \sin \psi [(e_{2X} + e_{1Y}) \cos \psi$$

$$+ (e_{3X} + e_{2Y}) \sin \psi] \}. \qquad (B3)$$

For a pure d-wave OP and $\psi \in [0, \pi/2]$, the angular dependence of $m_\perp$ [its normalization as given in Eq. (2.17)] is $f(\psi) = 3\sqrt{3} \cos \psi \sin \psi [\cos \psi - \sin \psi]$ and that for $m_\parallel$ it is $f_\parallel(\psi) = 3\sqrt{3}[\cos^3 \psi + \sin^3 \psi]$. While the angular modulation for $m_\parallel$ is somewhat smaller than that of $m_\perp$, the maximum of $m_\parallel$ is enhanced by a factor of $3\sqrt{3}$. This enhancement combined with ac measuring techniques[38] could facilitate examining the higher harmonics due to the nonlinear response.

APPENDIX C: FOURIER COMPONENTS FOR A NODELESS GAP

We give here the analytic expression for the harmonics $M_j(\psi)$, valid for a $d+is$ gap and $h_{dc} < h_{ac}$. Integration of Eq. (3.10) and substitution of $m_\perp$ from Eq. (3.7) yields

$$M_j(\psi) = \frac{2}{\pi} \frac{3\sqrt{3}}{h^2} \{ \cos \psi \sin \psi [\cos \psi (p_{1j}\Theta_1 + p_{3j}\Theta_3)$$

$$- \sin \psi (p_{2j}\Theta_2 + p_{4j}\Theta_4)]$$

$$+ 3\delta^2 [-\sin \psi (q_{1j}\Theta_1 + q_{3j}\Theta_3)$$

$$+ \cos \psi (q_{2j}\Theta_2 + q_{4j}\Theta_4)]$$

$$- 2\delta^3 [-\tan\psi(r_{1j}\Theta_1 + r_{3j}\Theta_3)$$

$$+ \cot\psi(r_{2j}\Theta_2 + r_{4j}\Theta_4)] \}, \quad j = 2,3, \qquad (C1)$$

where we have introduced the abbreviations

$$\Theta_{1,2} \equiv \Theta[a + b - h_{TX,Y}(\psi, \delta)],$$

$$\Theta_{3,4} \equiv \Theta[b - a - h_{TX,Y}(\psi, \delta)], \qquad (C2)$$

and a, b are replacing h_{dc} and h_{ac}, respectively. Since we work at a fixed maximum field ($h_{dc} + h_{ac} = \text{const}$), and $R = h_{dc}/h_{ac}$, $R \in [0,1)$, we set $a = (h_{dc} + h_{ac})R/(1+R)$, $b = (h_{dc} + h_{ac})/(1+R)$. The coefficients in Eq. (C1) for the 2ω component are

$$p_{i2} = \frac{b^2}{2} w_i + 2ab \sin w_i + \left(a^2 + \frac{b^2}{2} \right) \sin 2w_i$$

$$+ \frac{2}{3} \sin 3w_i + \frac{b^2}{8} \sin 4w_i, \quad i = 1,2, \qquad (C3a)$$

$$p_{k2} = \frac{b^2}{2} (w_k - \pi) + 2ab \sin w_k + \left(a^2 + \frac{b^2}{2} \right) \sin 2w_k$$

$$+ \frac{2}{3} \sin 3w_k + \frac{b^2}{8} \sin 4w_k, \quad k = 3,4, \qquad (C3b)$$

$$q_{i2} = \sin 2w_i, \quad i = 1, \ldots, 4, \qquad (C3c)$$

$$r_{i2} = \frac{4}{b} \sin w_i - \frac{4a}{b^2} w_i$$

$$+ \frac{2(2a^2/b^2 - 1)}{(b^2 - a^2)^{1/2}} \ln \left| \frac{(b-a)\tan(w_i/2) + (b^2 - a^2)^{1/2}}{(b-a)\tan(w_i/2) - (b^2 - a^2)^{1/2}} \right|,$$

$$i = 1, \ldots, 4, \qquad (C3d)$$

Those for the 3ω component are

$$p_{i3} = \frac{b^2}{2} \sin w_i + ab \sin 2w_i + \frac{2a^2 + b^2}{3} \sin 3w_i$$

$$+ \frac{ab}{2} \sin 4w_i + \frac{b^2}{10} \sin 5w_i, \quad i = 1, \ldots, 4, \qquad (C4a)$$

$$q_{i3} = \frac{2}{3} \sin 3w_i, \quad i = 1, \ldots, 4, \qquad (C4b)$$

$$r_{i3} = \frac{2}{b^3}[(4a^2-b^2)w_i - 4ab\sin w_i + b^2\sin 2w_i]$$

$$+ \frac{2a(-4a^2+3b^2)}{b^3(b^2-a^2)^{1/2}}\ln\left|\frac{(b-a)\tan(w_i/2)+(b^2-a^2)^{1/2}}{(b-a)\tan(w_i/2)-(b^2-a^2)^{1/2}}\right|,$$

$$i = 1,2, \qquad (C4c)$$

$$r_{k3} = \frac{2}{b^3}[(4a^2-b^2)(\pi-w_k) + 4ab\sin w_k - b^2\sin 2w_k]$$

$$- \frac{2a(-4a^2+3b^2)}{b^3(b^2-a^2)^{1/2}}\ln\left|\frac{(b-a)\tan(w_k/2)+(b^2-a^2)^{1/2}}{(b-a)\tan(w_k/2)-(b^2-a^2)^{1/2}}\right|,$$

$$k = 3,4, \qquad (C4d)$$

where $w_{1,2,3,4}$ denote possible values of ωt for which $|h(t)| = h_{TX,Y}$. The integral in Eq. (3.9) can be replaced by integrals over intervals $\omega t \in [0,w_i]$, $i=1,2$ and $\omega t \in [w_j,\pi]$, $j=3,4$. For example, w_1 and w_3 are the limits for contribution of quasiparticle jets along X axis and w_2 and w_4 those for jets along the Y axis. They can be expressed as

$$w_{1,2} = \cos^{-1}\left[\left(\frac{h_{TX,Y}-a}{b}-1\right)\Theta_{1,2}+1\right],$$

$$w_{3,4} = \cos^{-1}\left[\left(\frac{-h_{TX,Y}-a}{b}-1\right)\Theta_{3,4}-1\right], \qquad (C5)$$

for a pure d-wave gap, $w_i = \cos^{-1}(-a/b)$, $i=1,2,3,4$. The previously given expressions for $M_j(\psi)$, $j=2,3$, can then be used [see Eq. (3.10)] to obtain M_2^4, M_3^4, the $\pi/2$ angular Fourier components of the 2ω and 3ω signals of the transverse magnetic moment.

---

*Present address: Physics Dept., University of Maryland, College Park, MD 20742. Electronic address: izutic@physics.spa.umn.edu

†Electronic address: otvalls@tc.umn.edu

[1] J. F. Annett, N. Goldenfeld, and A. J. Leggett, in *Physical Properties of High Temperature Superconductors V*, edited by D. M. Ginsberg (World Scientific, Singapore, 1996).

[2] D. J. Scalapino, Phys. Rep. **250**, 331 (1995).

[3] J. R. Kirtley *et al.*, Nature (London) **373**, 225 (1995).

[4] D. J. Van Harlingen, Rev. Mod. Phys. **67**, 515 (1995).

[5] P. Kumar and P. Wölfle, Phys. Rev. Lett. **59**, 1954 (1987).

[6] J. A. Sauls, Adv. Phys. **43**, 113 (1994).

[7] Y. Nakatawa and K. Kanoda, Phys. Rev. B **55**, 8670 (1996).

[8] K. Kanoda *et al.*, Phys. Rev. Lett. **65**, 1271 (1990).

[9] H. Mayaffre *et al.*, Phys. Rev. Lett. **75**, 4122 (1995).

[10] K. A. Müller, Nature (London) **377**, 133 (1995).

[11] S. R. Bahcall, Phys. Rev. Lett. **76**, 3634 (1996).

[12] M. Fogelström *et al.*, Phys. Rev. Lett. **79**, 281 (1997).

[13] M. Covington *et al.*, Phys. Rev. Lett. **79**, 277 (1997).

[14] K. A. Kouznetsov *et al.*, Phys. Rev. Lett. **79**, 3050 (1997).

[15] K. A. Musaelian *et al.*, Phys. Rev. B **53**, 3598 (1996).

[16] W. Xu, W. Kim, Y. Ren, and C. S. Ting, Phys. Rev. B **54**, 12 693 (1996).

[17] N. Schopohl and O. V. Dolgov, Phys. Rev. Lett. **80**, 4761 (1998).

[18] D. F. Agterberg, T. M. Rice, and M. Sigrist, Phys. Rev. Lett. **78**, 3374 (1997).

[19] K. Ishida *et al.*, Phys. Rev. B **56**, 505 (1997).

[20] S. K. Yip and J. A. Sauls, Phys. Rev. Lett. **69**, 2264 (1992).

[21] B. P. Stojković and O. T. Valls, Phys. Rev. B **51**, 6049 (1995).

[22] D. Xu, S. K. Yip, and J. A. Sauls, Phys. Rev. B **51**, 16 233 (1995).

[23] I. Žutić and O. T. Valls, Phys. Rev. B **54**, 15 500 (1996).

[24] I. Žutić and O. T. Valls, J. Comput. Phys. **136**, 337 (1997).

[25] I. Žutić and O. T. Valls, Phys. Rev. B **56**, 11 279 (1997).

[26] P. A. Lee and X.-G. Wen, Phys. Rev. Lett. **78**, 4111 (1997).

[27] At T near T_c and for a static magnetic field, the effect of a $d+s$ energy gap on the nonlinear magnetization is studied in J. J. Betouras and R. Joynt, Phys. Rev. B **57**, 11 752 (1998).

[28] The nonlinear magnetic response in a static magnetic field and a mixed state is discussed by M. H. S. Amin *et al.*, Phys. Rev. B **58**, 5848 (1998).

[29] T. Dahm and D. J. Scalapino, J. Appl. Phys. **81**, 2002 (1997); Appl. Phys. Lett. **69**, 4248 (1996).

[30] F. London, *Superfluids* (Wiley, New York, 1950), Vol. 1.

[31] T. P. Orlando and K. A. Delin, *Foundations of Applied Superconductivity* (Addison-Wesley, Reading, MA, 1991).

[32] We assume here a cylindrical (not necessarily isotropic) FS. This is appropriate for unconventional layered superconductors. As shown in Ref. 23, inclusion of a noncylindrical three-dimensional FS introduces only a small correction.

[33] For an anisotropic FS surface some care has to be taken: at the nodal position s_n, the density of states $n(s_n)$ is not necessarily equal to the average value n_{iso} at each node we define $N_{fn} \equiv N_f n(s_n)/n_{iso}$.

[34] D. A. Bonn *et al.*, Phys. Rev. B **47**, 11 314 (1993).

[35] P. J. Hirschfeld, W. O. Putikka, and D. J. Scalapino, Phys. Rev. B **50**, 10 250 (1994).

[36] A. M. Goldman and A. Bhattacharya (private communication).

[37] It is simple to extend the solution to arbitrary thickness, as shown in Refs. 21,22,25.

[38] A. Bhattacharya (private communication).

[39] V. G. Kogan, Phys. Rev. B **38**, 7049 (1988); V. G. Kogan and J. R. Clem, *ibid.* **24**, 2497 (1981).

[40] D. Zech *et al.*, Phys. Rev. B **54**, 12 535 (1996).

[41] K. Maki and M. T. Béal-Monod, Phys. Rev. B **55**, 11 730 (1997).

[42] For our purposes there is no distinction between a $d+is$ and the $s+id$ gap considered in Ref. 25 as we discuss results which only depend on the absolute value of the OP.

[43] G. Kotliar, Phys. Rev. B **37**, 3664 (1988).

[44] Q. P. Li, B. E. Koltenbac, and R. Joynt, Phys. Rev. B **48**, 437 (1993).

[45] M. Sigrist, D. B. Bailey, and R. B. Laughlin, Phys. Rev. Lett. **74**, 3249 (1995).

[46] A. V. Balatsky *et al.*, Phys. Rev. Lett. **80**, 1972 (1998).

[47] R. Movshovich *et al.*, cond-mat/9709061 (unpublished).

[48] The normalization factor is the angular $\pi/2$ Fourier component of the normalized angular dependence for a pure d wave $[1/(3\sqrt{3})\cos\psi\sin\psi(\cos\psi-\sin\psi)]$, very approximately equal to unity.

[49] A. M. Goldman (private communication).

[50] I. Žutić and O. T. Valls, J. Appl. Phys. **83**, 6800 (1998).